VIP Core/Shell Nanoparticles

DOI: 10.1002/ange.201004287

Core-Protected Platinum Monolayer Shell High-Stability Electrocatalysts for Fuel-Cell Cathodes**

*Kotaro Sasaki, Hideo Naohara, Yun Cai, Yong Man Choi, Ping Liu, Miomir B. Vukmirovic, Jia X. Wang, and Radoslav R. Adzic**

For platinum-based catalysts, the requirements for durability and activity are heightened by the need to minimize platinum content, given its limited availability and high price. Furthermore, durability is particularly critical for fuel-cell cathodes because of the highly aggressive conditions, namely low pH, dissolved molecular oxygen, and the high positive potentials at which they operate. The durability of the existing platinum catalysts is unsatisfactory. Platinum nanoparticles (Pt NPs) can dissolve and redeposit on other Pt NPs.[1–3] Furthermore, Pt can deposit in the membrane by the reduction of Pt^{2+} by H_2 diffusing from the anode (hydrogen crossover). The major dissolution of these catalysts occurs under potential cycling regimes, which for example happen during the stop-and-go driving of electric cars. The consequent gradual decline in performance during operation, mainly caused by the loss of the electrochemical surface area (ECSA) of Pt NPs at the cathode, impedes the commercialization of low-temperature fuel cells. The lifetime required by the Department of Energy (DOE) for these catalysts is 5000 h, a goal that could be met only with thicker Pt layers[4] or larger particles[3] that can sustain sizeable Pt dissolution losses. These particle types suffer from drawbacks of high price and low Pt mass activity. Herein, we describe the mechanism of stabilization of new core/shell electrocatalysts illustrated by development of Pd and Pd_9Au_1 alloy core/Pt monolayer shell electrocatalysts with high activity and the very high stability that can facilitate their use in automotive fuel cells. We present an understanding of their properties that firmly establishes the concept of Pt monolayer catalysts that can address the future challenges of limited Pt resources.[5] The concept is applicable for similar applications of other noble metals, and is demonstrated by our findings from accelerated fuel-cell tests of the electrocatalyst stability during 100000 and 200000 potential cycles with $Pt_{ML}/Pd/C$ and $Pt_{ML}/Pd_9Au_1/C$, respectively. The data illustrate that the Pd core protects the Pt shell from dissolution. After 100000 or 200000 potential cycles, the electrocatalysts showed a small loss of ECSA and of catalytic activity, and a negligible loss of Pt. Under the same conditions, Pt/C catalysts suffer very large losses.

PtML/Pd/C electrocatalysts were synthesized by galvanic displacement by a Pt monolayer of a Cu monolayer deposited on Pd cores at underpotentials[6] (See the Experimental Section). The Z contrast images from high-angle annular dark field (HAADF) scanning transmission electron microscopy (STEM) show bright shells on relatively darker nanoparticles (Figure 1 a,b), signifying the formation of a core/shell structure; that is, a Pt monolayer shell ($Z = 78$) on a Pd NP core ($Z = 46$).[7,8] Figure 1 c,d depicts the line-profile analysis using STEM/energy dispersive spectroscopy (EDS), revealing the distribution of Pt and Pd components in a single nanoparticle. The lower Pt intensity at the center than at the Pd NP edges

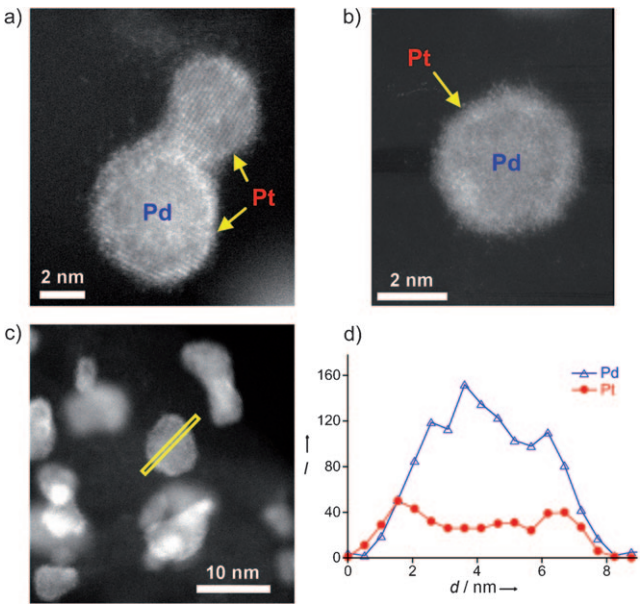

Figure 1. a–c) HAADF images of the sample of Pt monolayer shell on a Pd core nanoparticle, the $Pt_{ML}/Pd/C$ electrocatalyst, obtained in a 200 mg scaled-up synthesis. d) Distribution of components in a $Pt_{ML}/Pd/C$ nanoparticle in (c) obtained by a line-scan analysis using EDS.

[*] Dr. K. Sasaki, Dr. Y. Cai, Dr. Y. M. Choi, Dr. P. Liu, Dr. M. B. Vukmirovic, Dr. J. X. Wang, Dr. R. R. Adzic
Chemistry Department, Brookhaven National Laboratory
Upton, NY 11973 (USA)
Fax: (+1) 631-344-815
E-mail: adzic@bnl.gov
Dr. H. Naohara
Toyota Motor Corporation, Fuel Cell System Development Division
Susono, 410-1193 (Japan)

[**] This work was carried out at Brookhaven National Laboratory under contract no. DE-AC02-98CH10886, with the U.S. Department of Energy, Office of Science, and supported by its Division of Chemical Sciences, Geosciences, and Biosciences, and its Division of Materials Sciences and Engineering, within the Office of Basic Energy Sciences, and Toyota Motor Corporation. We thank the National Energy Research Scientific Computing (NERSC) Center, the Center for Functional Nanomaterials at Brookhaven National Laboratory, and Prof. M. C. Lin for CPU time. Work at the NSLS was supported by the DOE BES grant DE-FG02-03ER15688. We thank Hugh Isaacs and Radoslav Atanasoski for stimulating discussions.

Supporting information for this article is available on the WWW under http://dx.doi.org/10.1002/anie.201004287.

demonstrate the formation of a core(Pd)/shell(Pt) structure. Analyzing the atomic ratio of Pt and Pd and assuming that the height of Pd NP (normal to the picture) is equal to its width (8 nm) leads to the conclusion that the Pt shell is a monolayer. Figure 2 gives the results of the accelerated fuel-cell stability

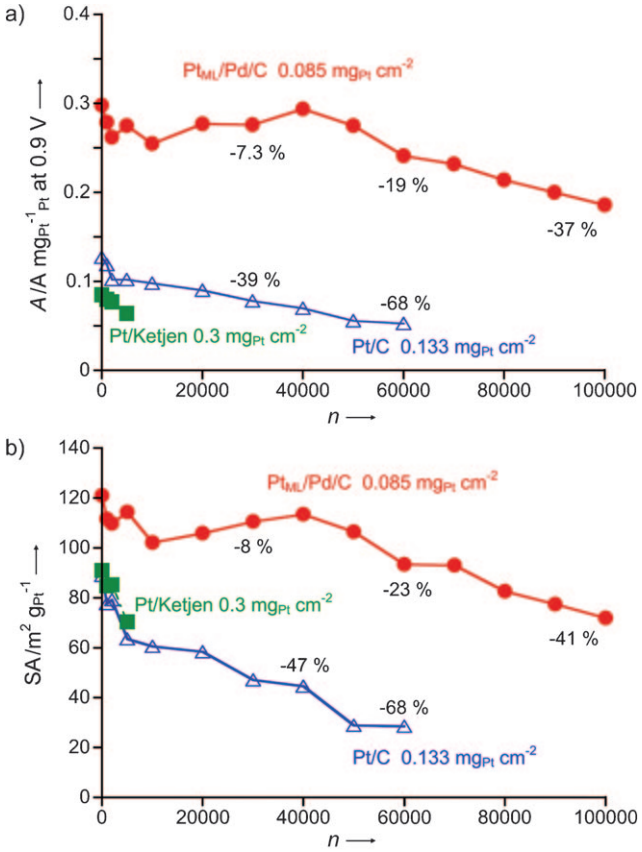

Figure 2. The Pt mass activity *A* for the ORR as a function of the number of potential cycles *n* during fuel cell testing of the PtML/Pd/C electrocatalyst. The limits of the potential cycle were 0.7 and 0.9 V (RHE), with a 30 s dwell time at 80 °C. The results with Pt/C and Pt/Ketjen carbon catalysts are shown for comparison. b) The electrochemical surface area (SA) of the three catalysts as a function of number of potential cycles.

tests of the PtML/Pd/C electrocatalyst by plotting Pt mass activity as a function of the number of potential cycles. The test involved potential step cycling between 0.7 and 0.9 V with a 30 second dwell time at 80 °C (see the Experimental Section). All potentials are given with respect to the reversible hydrogen electrode (RHE). After 100000 cycles, the Pt mass activity was decreased 37 %, indicating the excellent durability of this electrocatalyst. For comparison, the Pt mass activity of two commercial Pt/C catalysts is about three times smaller than that of the PtML/Pd/C electrocatalyst. Thus, after 60000 potential cycles, Pt/C had lost almost 70 % of its activity, compared with less than 20 % for PtML/Pd/C; the activity of Pt/Ketjen black carbon had fallen more than 40 % after only 10000 cycles. It is particularly important and informative that at 60000 cycles, the Pt mass activity of PtML/Pd/C catalyst increased from the initial threefold to fivefold enhancement over that of Pt/C. This fact clearly illustrates the superior stability of the PtML/Pd/C (Table 1). Figure 2b shows the electrochemical surface area, calculated from H-adsorption charges, of the three catalysts as

Table 1: Platinum mass activity, electrochemical surface area, specific activity, and particle size for electrocatalysts before and after potential cycling tests.[a]

Sample	Pt mass activity [$mA\,\mu g^{-1}$]	ECSA [$cm^{-2}\,\mu g^{-1}$]	Specific activity [$mA\,cm^{-2}$]	Size [nm]
Pt initial	0.13	0.90	0.14	3.5
Pt 6×10^4	0.05	0.27	0.19	
Pt_{ML}/Pd initial	0.30	1.20	0.25	4.0
Pt_{ML}/Pd 6×10^4	0.24	0.93	0.26	–
Pt_{ML}/Pd 1×10^5	0.19	0.70	0.27	3.6
Pt_{ML}/Pd_9Au_1 initial	0.30	0.60	0.5	5.0
Pt_{ML}/Pd_9Au_1 2×10^5	0.20	0.20	1.0	3.8

[a] All of the electrocatalysts are carbon-supported nanoparticles; the number of cycles is indicated after the catalyst symbol.

a function of the number of potential cycles. Comparing these two sets of data (Figure 2a,b) highlights the remarkable parallelism between the potential cycling dependence of the electrochemical surface area and the Pt mass activity for all three catalysts. With our PtML/Pd/C catalyst, we found that after 100000 potential cycles, a considerable amount of Pd had migrated. It was oxidized, dissolved as Pd^{2+}, and diffused out of the cathode catalyst layer into the Nafion membrane. The Pd^{2+} was reduced by H_2 diffusing from anode and deposited in the membrane and on the anode. In the membrane, it forms a Pd "band" (Figure 3b) similar to the band that resulted in other catalysts from dissolution of Pt under potential cycling regimes.[9] Some Pd remained in the cathode catalyst layer, whilst a negligible amount of Pt was detected in the membrane. Comparison of Figure 3a (before potential cycling) with Figure 3b (after potential cycling) showed that, despite a considerable loss of Pd, the core/shell structure of the Pt_{ML}/Pd/C catalyst still exists after 100000 potential cycles between 0.7 and 0.9 V. The shell integrity was verified by the HAADF images with a EDS line analysis (Figure 3c,d). Comparing these data with Figure 1c,d confirms this loss of Pd. The ratio of the peak intensities for Pd and Pt is smaller after potential cycling (Figure 3) than before (Figure 1), which corroborates these assertions. The evidence that the Pt monolayer stays on the surface of nanoparticles, and that the core/shell nanocatalyst is more active and stable than pure Pt, is very important for future catalysis. It opens up a broad opportunity for the design of new catalysts with monolayer amounts of noble metals. Potential cycling affects the particle size distribution and causes an increase of mass activity of the Pt(ML)/Pd/C electrocatalyst. The latter point suggests that the effect of the Pd support on a Pt monolayer remains intact and that additional changes in the core/shell

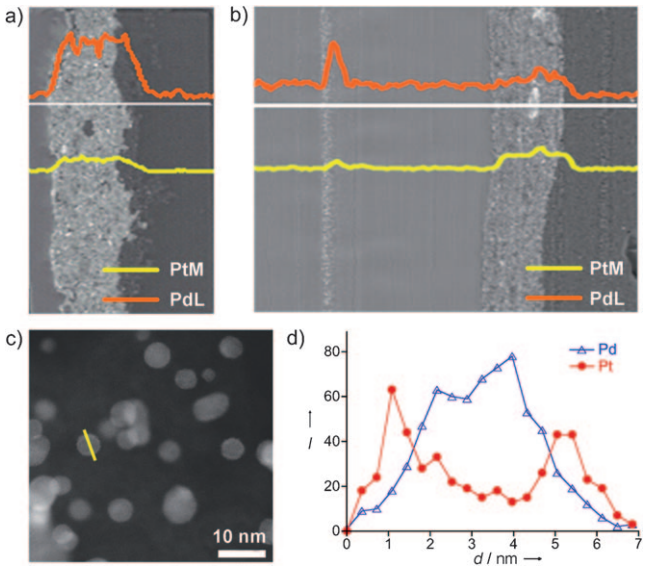

Figure 3. Cross-section of the membrane electrode assembly (MEA) showing the concentration profiles for Pd and Pt before (a) and after 100 K potential cycles (b). c) HAADF image of PtML/Pd/C particles and d) the distribution of a Pt monolayer on a Pd core/shell nanoparticle, obtained by line analysis of EDS after the test.

interaction may have occurred. The particle size distribution before and after potential cycling had the mean value of (4.0 ± 1.2) nm, and (3.6 ± 1.4) nm, respectively (Supporting Information, Figures S1a, S2b, respectively).

The dissolution of Pt is a major pathway of degradation of the Pt electrocatalysts in low-temperature fuel cells. Pt is likely lost through its dissolution at relatively high potentials (greater than 0.8 V, where PtOH is formed). The solubility of Pt as a function of electrode potential was demonstrated for several nanoparticles.[1,10,11] Dissolution of submonolayer–monolayer amounts of Pt is considered important part of the Pt dissolution mechanism.[12] Apparently, submonolayer dissolution processes deviate from equilibrium thermodynamic considerations.[13] Indeed, the non-Nernstian behavior of measured Pt dissolution indicates that significant amounts of Pt and of the Pt surface area can be lost by dissolving only the first monolayer.[3] Thus, we would expect the stability of a Pt_{ML}/Pd/C electrocatalysts to persist only for a short time under potential cycling regimes. The difference between this prediction and the stability we demonstrated during more than 100 000 potential is striking.

The pronounced effect of a Pd core on the activity of a Pt monolayer shell is in agreement with the top position (the highest activity) of this couple in the "volcano" plot, which is the correlation established for the oxygen reduction reaction (ORR) kinetics for a Pt monolayer on the six single-crystal surfaces.[14] Not only did the Pd core efficiently assure the long-term stability of the monolayer-thick Pt shell, but it increased the Pt monolayer activity for the ORR by causing it to contract slightly that, in turn, decreased its reactivity by lowering its d-band center energy[15] and reducing the bond strength of adsorbed oxygen intermediates.[16,17] These effects decrease the bonding of OH and O to Pt that inhibits the ORR kinetics[18] and also stabilize Pt against oxidation and dissolution. In addition to shifting positively the Pt oxidation, the following mechanism facilitates the remarkable stability of Pd-supported Pt monolayer electrocatalyst as oxygen cathode during potential cycling. Pd is a slightly more reactive metal than Pt, with a lower standard electrochemical potential; direct Pd dissolution ($Pd \rightarrow Pd^{2+} + 2e^-$, $U^0 = 0.92$ V) occurs at slightly lower potentials than Pt (1.19 V). Thus, when the positive potential of the Pt/Pd/C core/shell nanoparticle rises to near the reversible electrochemical potential of Pd owing to an exposure to fluctuating fuel-cell voltage, the Pd may be oxidized to Pd^{2+} and diffuse through any imperfection (puncture) in a Pt monolayer. This reaction will impede further increase of potential in an operating fuel cell, or at least minimize it. As an ideal, puncture-free monolayer is difficult to generate, the Pd core could well establish contact with the electrolyte, where it would be oxidized slowly when its dissolution potential is reached. After prolonged potential cycling and significant dissolution of Pd, the Pt monolayer shell will undergo a small contraction that will make it less reactive[15] and will raise its existing high stability and dissolution resistance. Such contraction will cause a decrease in particle size to form a more stable structure. As a result, the excess of Pt atoms from a monolayer shell of larger particles will form a partial bilayered structure. A substantial dissolution of Pd may cause the formation of hollow particles that are not easily confirmed by experimental techniques, but allowed for by DFT calculations. Therefore, in addition to increasing stability of Pt by contracting its lattice, Pd exerts a certain degree of cathodic protection on Pt.

Our EXAFS and electron-energy-loss spectroscopy (EELS) data verify the protection of a Pt shell by a Pd core and the significant loss of Pd. Figure 4 presents the ex situ EXAFS spectra of the Pt L3 edge obtained from the Pt/Pd/C electrocatalyst after a fuel-cell test of 60 000 potential cycles, together with the in situ EXAFS spectra measured at a potential of 0.41 V before the cycle test. We have confirmed the formation of a Pt monolayer on the Pd NP surface of the sample prior to the potential cycles using in situ EXAFS. After the potential cycles, the signal of Pd K edge becomes too small to fit Pt L3 and Pd K data concurrently and to allow the atomic structures to be examined in detail. However, the general appearance of both Pt spectra are similar (except for $k^2 < 2$ Å^{-1}, which is due to the oxidation of Pt), pointing to the near-retention of the structure of Pt shells throughout 60 000 cycles. Figure 4b shows the EELS spectra of the Pd M edge from Pt_{ML}/Pd/C NPs before and three individual particles after the same test. The post-test intensities of the Pd M edge are much lower than that from a Pt_{ML}/Pd/C NP with 4.2 nm diameter before the test (red line); we note that the EELS and EDX revealed no marked loss in Pt intensity after cycling.

We carried out DFT calculations to further elucidate the observed behavior of Pt_{ML}/Pd/C electrocatalysts. To simulate the Pt Pd NP after Pd dissolution, we constructed three types of sphere-like nanoparticle models based on a truncated octahedron (see Figure 5). To reduce computational time, only half of the nanoparticle was considered. As shown in Figure 5d, the 1ML Pt dissolution potentials from Pt and

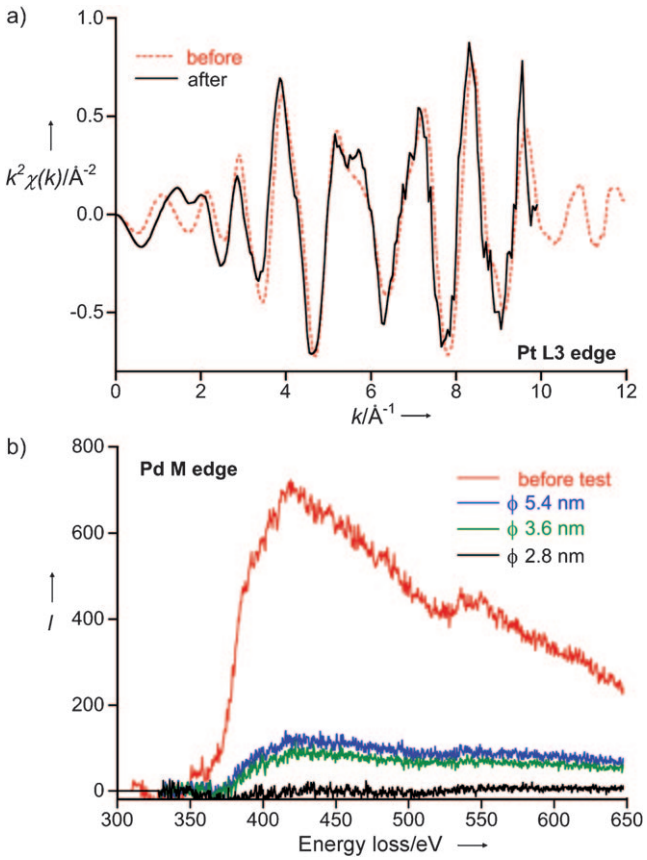

Figure 4. a) EXAFS spectra of the $Pt_{ML}/Pd/C$ electrocatalyst before and after the MEA test. k^2-weighted EXAFS data of Pt L3 edge from $Pt_{ML}/Pd/C$ electrocatalyst before and after 60000 potential cycles between 0.7 V and 0.9 V at 80 °C. b) EELS spectra of the Pd M edge from $Pt_{ML}/Pd/C$ nanoparticles beforehand (red trace) and from three particles (diameters indicated in the graph) after the 60000 potential cycle test.

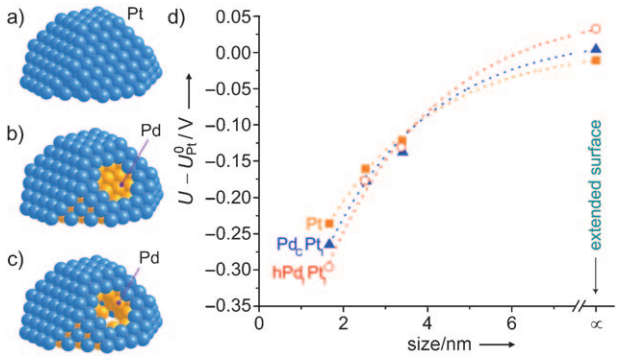

Figure 5. Surface models for the nanoparticles: a) pure Pt nanoparticles (Pt in our notation), b) Pt_{ML}/Pd with a solid Pd core (Pd_CPt_1), and c) Pt_{ML}/Pd with only a 1 ML Pd inner core (hPd_1Pt_1). d) Predicted dissolution potentials of a 1 ML Pt shell from nanoparticles and extended surfaces of Pt, Pd_CPt_1, and hPd_1Pt_1 as a function of particle sizes. The particle sizes studied are approximately 1.7 nm, 2.5 nm, and 3.4 nm.

PtPd NPs vary with the particle size. With the size of around 1.7 nm, pure Pt displays the higher dissolution potential then Pd_CPt_1 and hPd_1Pt_1 core/shell nanoparticles. According to our calculated binding energies, the Pt shell/Pd core interaction is slightly weaker than the Pt shell/Pt core interaction (that is, −4.72 and −4.78 eV/Pt atom, respectively). However, it would be expected that the Pd core, with a higher-lying d band, should provide a stronger binding to the Pt shell than the Pt core.[15] This effect is associated with less contraction, which is observed for the pure Pt NP than that for Pd_CPt_1 (3.6 and 4.0%, respectively). According to previous studies,[15,19] the contraction on a metal surface or nanoparticle leads to a deactivation, and therefore in the current case the weaker Pt shell/Pd core interaction. Furthermore, a careful structure analysis showed that hPd_1Pt_1 with the 1.7 nm size is slightly collapsed inward, leading to a surface contraction of 4.5% and a circa 0.06 eV/Pt atom decrease in binding energy compared to Pd_CPt_1. Our calculations for the 1.7 nm nanoparticles disagree with our experimental observation (Figure 2), which is most likely due to the considerable difference between the 1.7 nm particle size of our model and the size determined from experiment (ca. 4 nm). For a particle size increase to approximately 2.5 nm and 3.4 nm, we found that the surface contractions decrease and the dissolution potentials of Pt, Pd_CPt_1, and hPd_1Pt_1 increase (Figure 5d). The DFT results show that hPd_1Pt_1 (4.3% for 2.5 nm and 4.2% for 3.4 nm) exhibits more surface contraction than those of Pt (3.1% for 2.5 nm and 2.8% for 3.4 nm) and Pd_CPt_1 (3.3% for 2.5 nm and 2.9% for 3.4 nm), which leads to a shrinkage of the nanoparticle of Pd_CPt_1 (2.54 nm versus 2.51 nm and 3.41 nm versus 3.37 nm, respectively). This result clearly supports the experimental finding of a decrease in size of PtPd NPs before and after potential cycling (Supporting Information, Figure S2a,b). According to our previous study on the ORR on PtPd NPs,[19] the surface contraction introduced by using a Pd core is able to decrease the bonding of OH and O to Pt, which inhibits the ORR kinetics. Considering the sequence of the surface contraction on Pt, Pd_CPt_1, and hPd_1Pt_1, it would also be expected that the weakest core/shell interaction is for hPd_1Pt_1, as shown in the case of 1.7 nm. However, the corresponding binding energy of the Pt shell is almost identical (ca. −4.9 eV/Pt atom for 2.5 nm and about −5.0 eV/Pt atom for 3.4 nm) and the difference in dissolution potential among the three kinds of nanoparticles is negligible. With the larger sizes, the Pt shell of hPd_1Pt_1 is not collapsed inward, and the shape is maintained like Pd_CPt_1. There are two factors that possibly affect the Pd core/Pt shell interaction: one is the surface contraction and the other is the binding activity of the Pd core. Considering the former factor, the core/shell interaction should be weakened by forming hPd_1Pt_1, as mentioned above. However, the Pd layer in hPd_1Pt_1 that directly interacts with the Pt shell has the lower coordination than that in Pd_CPt_1, which is more active and able to bond Pt more strongly.[15] It seems that these two factors operate in an opposite way and result in a comparable core/shell interaction (Figure 5d). Due to the high CPU demand, we considered using the extended surfaces as an extreme case to model the large nanoparticles. As shown in Figure 5d, all of the nanoparticles are more prone to dissolution than each corresponding extended surface. 1ML Pt on a one-layer Pd(111) representing hPd_1Pt_1 has the highest dissolution potential among the nanoparticles studied. The surface contractions of the two PtPd systems on the

extended surfaces are the same (ca. 0.4%), which is much smaller than those of the nanoparticles we studied. Again, the lower-coordinated Pd core in hPd_1Pt_1 provides a stronger binding to the Pt shell than those in the cases of Pd_CPt_1 and Pt (−5.32 eV/Pt atom for hPd_1Pt_1, −5.26 eV/Pt atom for Pd_CPt_1, and −5.23 eV/Pt atom for Pt), which stabilizes the active Pt on the surface. Overall, the DFT calculations show that the relative shift in the dissolution potential depends strongly on the particle size. For both Pt and PtPd NPs, the larger particles display a higher dissolution potential than smaller ones. Compared to Pt and Pd_CPt_1, the partially hollow-structure hPd_1Pt_1 NPs with a certain size (>2.5 nm; Figure 5d) formed by the dissolution of Pd from the punctures exhibit the strongest binding to the Pt shell and the highest dissolution potentials. Note that the present calculations do not describe the kinetics observed experimentally, where the Pt dissolution potentials are not reached until the Pd dissolution is complete; however, it does capture the thermodynamics features, where the partial dissolution of Pd leads to the strengthened core/shell interaction and therefore a stabilized Pt shell.

We improved further the stability and activity of the Pt_{ML}/Pd/C monolayer electrocatalyst by alloying Pd with a small amount of gold to obtain a Pd_9Au_1 alloy core. The results provide additional evidence for the role of the Pd core in stabilizing a Pt monolayer. In agreement with recent studies,[20] our results show that alloying of Pd with Au (Supporting Information, Figure S3) causes a positive shift of Pd oxidation potential and less PdOH formation, as shown by voltammetry (Supporting Information, Figure S4) and in situ EXAFS studies (Supporting Information, Figure S5). The changes in coordination number of Pd–O demonstrate this tendency very clearly. It has a considerably weaker potential dependence for Pd_9Au_1 than for Pd, indicating the less-oxidized Pd in the alloy (Supporting Information, Figure S5). Consequently, the alloy increases the stability of the $Pt/Pd_9Au_1/C$ electrocatalyst, which was verified in the test involving 200000 potential cycles from 0.6 to 1.0 V at the sweep rate of 50 mV s^{-1}. We recently discussed the stabilization of Pt NPs by Au clusters under potential cycling conditions,[21] which underlines the extent of the effects of surface modification. Figure 6a shows the Pt mass activity of the $Pt_{ML}/Pd_9Au_1/C$ electrocatalyst as a function of the number of potential cycles from 0.7 to 0.9 V. In 200000 cycles, the Pt mass activity decreased about 30%, which is an excellent stability. The DOE target for 30000 potential cycles of the same procedure is a loss of 40%. For comparison, the mass activity of commercial Pt/C catalyst is given, showing a terminal loss below 50000 cycles. Figure 6b shows the distribution of Pt, Au, and Pd in the catalyst nanoparticle after the test. The potential cycling caused a decrease of Pd content and a negligible change of the content of Pt and Au. This observation is corroborated by analyzing the cross-section of the MEA and the concentration profiles of Pd, Pt, and Au in Figure 6c,d. As in Figure 3, the "band" of Pd (center) is a consequence of Pd dissolution and reduction of Pd^{2+}. The cathode catalyst $Pt_{ML}Pd_9Au_1$ is at right side. The average particle size, determined from the TEM data, before and after testing was (5.0 ± 1.7) nm and (3.8 ± 1.2) nm, respectively. This behavior is similar to that observed with the Pt_{ML}Pd/C catalyst, except for the higher stability of the $Pt_{ML}/Pd_9Au_1/C$ electrocatalyst. A dramatic increase of stability is created by simple alloying of the core with Au that facilitated 200000 potential cycles from 0.6 to 1.0 V, compared with 100000 from 0.7 to 0.9 V with a core without Au.

Therefore, in these Pd- or Pd_9Au_1-supported Pt monolayer core/shell nanoparticles, the core increases the stability of the shell by shifting positively its oxidation potential, and by preventing the cathode potential reaching values at which Pt dissolution takes place. The latter is realized by the slow oxidation of the Pd core that impedes excursions of the cathode potentials to high values. Increasing particle size has an additional effect in increasing stabilization. No loss of Pt was observed, whereas a substantial loss of Pd caused a small

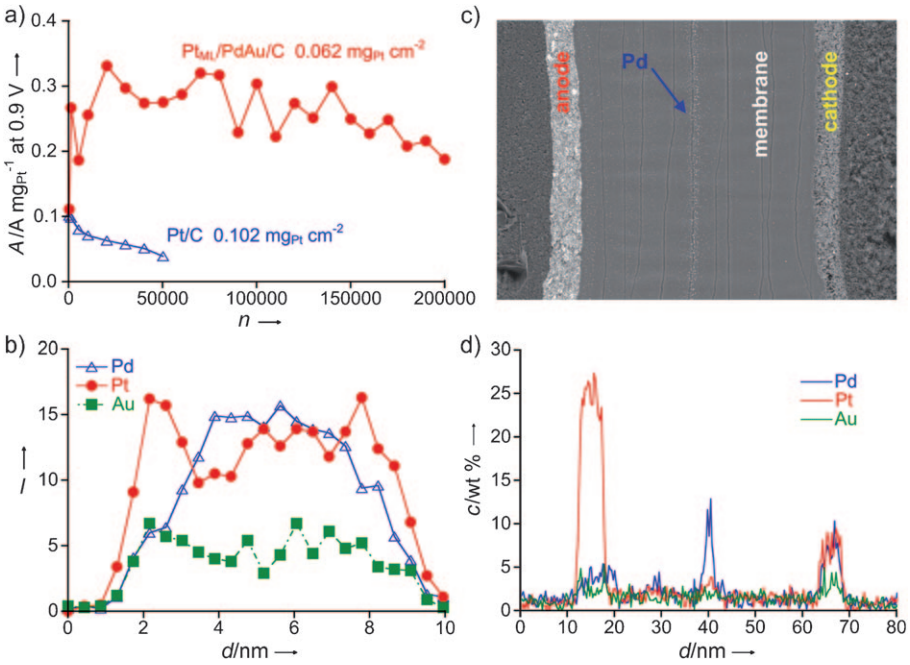

Figure 6. a) The Pt mass activity for the ORR as a function of the number of potential cycles during fuel-cell testing of the $Pt_{ML}/Pd_9Au_1/C$ and Pt/C electrocatalysts containing 0.062 $mg_{Pt}\,cm^{-2}$ and 0.102 $mg_{Pt}\,cm^{-2}$, respectively. The limits of the potential cycle were 0.6 and 1.0 V; sweep rate of 50 mV s^{-1}. b) The distribution of a Pt, Au, and Pd in the catalyst nanoparticle, obtained by line analysis of EDS after the test. c) Cross-section of the membrane electrode assembly (MEA) showing the Pt catalyst layer in the anode (left), the "band" of Pd (center), and the cathode catalyst $PtMLPd_9Au_1$ (right). d) Corresponding concentration profiles (*c* versus distance *d*) for Pt, Pd, and Au after the test.

decrease in the nanoparticle size. Our DFT calculations support the experimental data and indicate that hollow structures that can form under these conditions would have the highest dissolution potentials. In addition to developing the electrocatalysts that can facilitate automotive application of fuel cells, these findings indicate the broad applicability of the Pt monolayer catalysts and the possibility of extending this concept to the catalysts based on other noble metals.

Experimental Section

One batch-synthesis of 2 g of the Pt_{ML}/Pd/C catalyst was carried out using the galvanic displacement of a Cu monolayer by dissolved K_2PtCl_4. A Cu monolayer was obtained by underpotential deposition (UPD) of a Cu monolayer on the reduced surfaces of the Pd nanoparticles. Pd_9Au_1 alloy was synthesized using wet impregnation of XC-72 carbon by Pd and Au chlorides, dried, and reduced using $NaBH_4$ solution. Particles were characterized using standard methods. Structural studies were carried out using the high-angle annular dark field (HAADF), scanning transmission electron microscopy (STEM), electron energy-loss spectroscopy (EELS), and extended X-ray absorption fine structure (EXAFS) techniques.

A potential program was applied to the cell comprising the membrane electrode assembly using H_2 at the anode (counter electrode) and N_2 at the cathode (working electrode) at 150 kPa absolute pressure and 100% relative humidity (RH) at 80 °C. Single cells with a surface area of 25 cm^2 and a Nafion NRE211CS membrane (25 mm) was used. The accelerated stability test involved potential step cycling between 0.7 and 0.9 V with a 30 s dwell time with Pt_{ML}/Pd/C catalyst, whilst a linear potential sweep at a rate of 50 $mV\,s^{-1}$ was applied from 0.6 to 1.0 V with the Pt_{ML}/Pd_9Au_1/C catalyst. O_2 was injected in the cathode and polarization curves were obtained.

All DFT calculations were carried out using the Vienna ab initio simulation package.[22,23] We employed the generalized gradient approximation (GGA) using the revised Perdew–Burke–Ernzerholf (RPBE) functional[24] with the projector-augmented wave method (PAW)[25] to describe the exchange and correlation energies. To examine the dissolution potential of Pt atoms, we followed the previous work of Greeley and Nørskov.[26] Other details are given in the Supporting Information.

Received: July 14, 2010
Published online: October 7, 2010

Keywords: core/shell particles · fuel cells · monolayers · palladium · platinum

[1] P. J. Ferreira, G. J. la O, Y. Shao-Horn, D. Morgan, R. Makharia, S. Kocha, H. A. Gasteiger, *J. Electrochem. Soc.* **2005**, *152*, A2256 – A2271.
[2] "Dissolution and Stability of Platinum in Oxygen Cathodes": K. Sasaki, M. Sao, R. Adzic in *Polymer Electrolyte Fuel Cell Durability*, Springer Science, New York, **2009**.
[3] S. Chen, H. A. Gasteiger, K. Hayakawa, T. Tada, Y. Shao-Horn, *J. Electrochem. Soc.* **2010**, *157*, A82 – A97.
[4] M. K. Debe, A. K. Schmoeckel, Vernstrorn, R. Atanasoski, *J. Power Sources* **2006**, *161*, 1002 – 1011.
[5] R. R. Adžić, J. Zhang, K. Sasaki, M. B. Vukmirovic, M. Shao, J. X. Wang, A. U. Nilekar, M. Mavrikakis, J. A. Valerio, F. Uribe, *Top. Catal.* **2007**, *46*, 249 – 262.
[6] S. R. W. Brankovic, J. X. Wang, R. R. Adžić, *Surf. Sci.* **2001**, *474*, L173 – L179.
[7] C. P. Liu, R. D. Twesten, J. Murray Gibson, *Ultramicroscopy* **2001**, *87*, 79 – 88.
[8] D. Garcia-Gutierrez, C. Gutierrez-Wing, M. Miki-Yoshida, M. Jose-Yacaman, *Appl. Phys. A* **2004**, *79*, 481 – 487.
[9] H. A. Gasteiger, S. S. Kocha, B. Sompalli, F. T. Wagner, *Appl. Catal. B* **2005**, *56*, 9 – 35.
[10] Y. Shao-Horn, W. C. Sheng, C. Chen, P. J. Ferreira, E. F. Holby, D. Morgan, *Top. Catal.* **2007**, *46*, 285 – 305.
[11] R. M. Darling, J. P. Meyers, *J. Electrochem. Soc.* **2003**, *150*, A1523 – A1527.
[12] V. Komanicky, K. C. Chang, A. Menzel, N. M. Markovic, H. You, X. Wang, D. Myers, *J. Electrochem. Soc.* **2006**, *153*, B446 – B451.
[13] J. Greeley, M. Mavrikakis, *Nat. Mater.* **2004**, *3*, 810 – 815.
[14] J. Zhang, M. B. Vukmirovic, Y. Xu, M. Mavrikakis, R. R. Adzic, *Angew. Chem.* **2005**, *117*, 2170 – 2173; *Angew. Chem. Int. Ed.* **2005**, *44*, 2132 – 2135.
[15] B. Hammer, J. K. Nørskov, *Adv. Catal.* **2000**, *45*, 71 – 129.
[16] J. X. Wang, J. Zhang, R. R. Adzic, *J. Phys. Chem. A* **2007**, *111*, 12702 – 12710.
[17] A. U. Nilekar, M. Mavrikakis, *Surf. Sci.* **2008**, *602*, L89 – L94.
[18] J. X. Wang, N. M. Markovic, R. R. Adzic, *J. Phys. Chem. B* **2004**, *108*, 4127 – 4133.
[19] J. X. Wang, H. Inada, L. Wu, Y. Zhu, Y. M. Choi, P. Liu, W.-P. Zhou, R. R. Adzic, *J. Am. Chem. Soc.* **2009**, *131*, 17298 – 17302.
[20] M. Lukaszewski, A. Czerwinski, *J. Electroanal. Chem.* **2006**, *589*, 38 – 45.
[21] J. Zhang, K. Sasaki, E. Sutter, R. R. Adzic, *Science* **2007**, *315*, 220 – 222.
[22] G. Kresse, J. Hafner, *Phys. Rev. B* **1993**, *47*, 558 – 561.
[23] G. Kresse, J. Furthmüller, *Phys. Rev. B* **1996**, *54*, 11169 – 11186.
[24] B. Hammer, L. B. Hansen, J. K. Nørskov, *Phys. Rev. B* **1999**, *59*, 7413 – 7421.
[25] P. E. Blöchl, *Phys. Rev. B* **1994**, *50*, 17953 – 17979.
[26] J. Greeley, J. K. Nøskov, *Electrochim. Acta* **2007**, *52*, 5829 – 5836.

